Supplementary Information

Light-reconfigured waveband-selective diffraction device enabled by micro-patterning of a photoresponsive self-organized helical superstructure

Pei-zhi Sun,[a] Zhen Liu,[a] Wei Wang,[a] Ling-ling Ma,[b] Dong Shen,[a] Wei Hu,[b] Yanqing Lu,[b] Lujian Chen,[c] and Zhi-gang Zheng[a,b]

[a.] *Department of Physics, East China University of Science and Technology, No.130, Meilong Road, Shanghai, 200237, China.*

E-mail: zgzheng@ecust.edu.cn

[b.] *National Laboratory of Solid State Microstructures and College of Engineering and Applied Sciences, Nanjing University, Nanjing 210093.*

[c.] *Department of Electronic Engineering, School of Information Science and Engineering, Xiamen University, Xiamen 361005, China.*

Pre-photo-crosslinking

Generally, it is difficult to form a high resolution micro-pattern in a fluidic photoresponsive LC system through the photo-patterning due to the molecular diffusions and the long range interaction in such system. Photo-crosslinking is a facile and effective approach to suppress and weaken the aforementioned dynamic problems on account of the strong anchoring of polymer network on LC molecules, thus enabling the formation of microstructures. As mentioned in the main text, a pre-photo-crosslinking was implemented commonly by doping a small amount of photopolymerizable monomers and photoinitiator into the host CLCs and followed by a light irradiation at the proper conditions. Herein, the conventional commercial available liquid crystalline monomer, RM257, provided by Wilshire Tech., Inc., and a visible-light sensitive photoinitiator, Irgacure 784, provided by BASF, were adopted considering the solubility of the system and the effect of polymer stabilization. Different from the monomer system commonly used for polymer stabilization, herein the one-functionality acrylate monomer with short alkylene chain, such as the 2-ethylhexyl acrylate, which promoted the crosslinking density of polymer network, was removed to form a looser network, thereby keeping the satisfying phototuning performance as well as compressing the molecular movements. On the molecular geometry viewpoint, QL55 was a little larger than the RM257, which was supposed to result in the difficult movement of QL55 confined in polymer network formed by pure RM257 monomers.

The whole mixture was injected into a 5-μm thick anti-parallel alignment treated planar cell at 55°C (*i.e.*, isotropic state) and cooled to the room temperature (about 20 °C) with a slow rate of 0.1 °C/min controlled by a precise hot stage (Linkam LTS120E), followed by a light exposure with 480-nm light-emitted-diode (LED) source for about 30~40 min at the dark ambient. The output intensity of LED source was controlled as 2.5 mW/cm^2. Subsequently, the sample was irradiated by a UV mercury lamp (365 nm), with the intensity of 4.0 mW/cm^2, for detecting the light-tunable performance of the reflection band (Figure S1). It needs to be noticed that the monomer concentration played a pivotal role on the performances of phototuning and the formation of micro-patterns. The results exhibited the micro-patterns with unsharp boundaries in the case of low monomer concentration (4.0 wt%, Figure S2); a satisfying micro-pattern formed as the monomer concentration was high, however its phototuning property was degraded simultaneously. Herein, 6 wt% RM257 was a proper concentration for forming a better performance micro-pattern as mentioned in the main text.

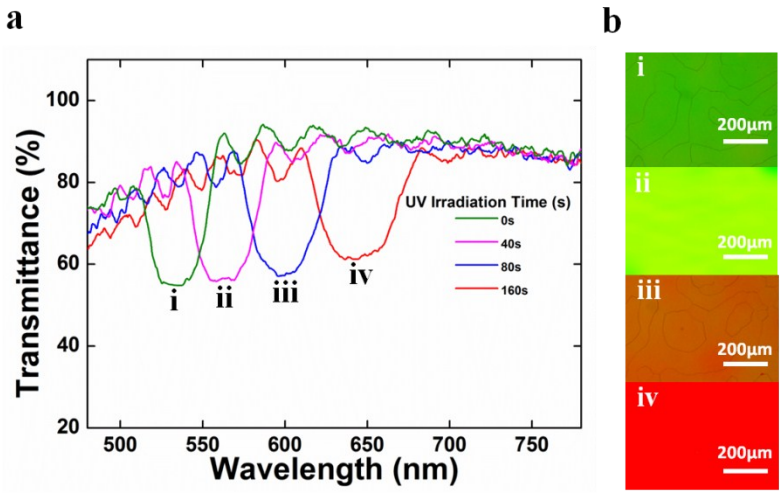

Fig. S1. Light manipulation of reflection band under UV-irradiation (365 nm, 4.0 mW/cm^2) after pre-photo-crosslinking. (**a**) Spectra detected at some certain irradiation time (The reflection band would shift no longer after 160s as the photoisomerization was finished under the UV exposure); and (**b**) their corresponding textures under the reflection-mode of polarizing optical microscope.

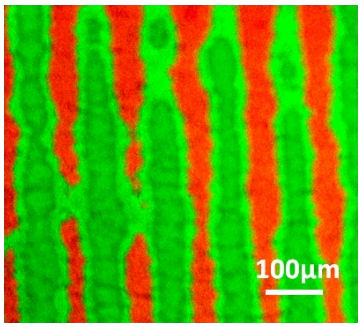

Fig. S2. Micrograph of the photo-patterned microstructure in the case of a weak pre-photo-crosslinking (4.0 wt% monomer). The unsharp boundary of the stripe pattern indicates a gradient pitch length caused by possible molecular diffusion and the long range interaction.

Helical twisting power

The HTP of chiral molecular switch QL55 in the initial, PSS_{UV}, and PSS_{vis} states were 34.5 μm^{-1}, 17.3 μm^{-1}, and 33.7 μm^{-1} respectively. These values were determined with the commonly used Grandjean-Cano wedge method, which has been presented in many literatures previously.[1,2] Regarding to the mixture in our experiment, provided that the HTPs for the mixed system, the chiral R811 and the chiral switch QL55 were $(HTP)_0$, $(HTP)_{811}$, and $(HTP)_{QL}$, respectively; the weight ratio of R811 and QL55 are denoted by C_{811} and C_{QL}, respectively; thus the following relationship was obtained,

$$(HTP)_0 = C_{811}(HTP)_{811} + C_{QL}(HTP)_{QL} \qquad \text{Eq. (S1)}$$

Herein, $C_{811}\times(HTP)_{811}$ was 1.949 μm^{-1}, C_{QL}=3 wt%, therefore $(HTP)_{QL}$ can be calculated through Eq. (S1) by testing $(HTP)_0$ through Grandjean-Cano wedge method. The Cano-wedge cell used for HTP testing was supported by Instec Co., Ltd. with an anti-parallel alignment treatment. The values of HTP in PSS_{UV} and PSS_{vis} states were tested respectively, by irradiating the sample confined in the Cano-wedge cell with UV and visible lights.

Photo-micro-patterning

The sample was triggered to photo stationary state (PSS_{UV}) after the irradiation of the UV lamp. Subsequently, the photo-micro-patterning was carried out by irradiating a photomask-covered CLCs sample with the collimated 532-nm laser (the sample at PSS_{UV} before the patterning). For example, a stripe-pattern was obtained after the light passed through a corresponding binary stripe photomask. To avoid the Fresnel reflection at the interfaces induced by the air-layer between photomask and LC cell, a thin refractive-index-matching layer (provided by Nikon) was coated on the contact surface firstly. The refractive-index of such layer, 1.510, was very close to the glass, 1.515.

Detection of diffraction patterns

The optical setup was shown in Figure S3. A linearly polarized probe beam was expanded after passing through a beam expander (**E**) composed by two lenses and a pinhole (diameter: 25 μm, provided by Newport Co. Ltd., USA). The expanded beam was transformed to the right-handed circularly polarized light by passing successively through a polarizer (**P**, transmission axis: 0°) and a quarter wave plate (**QWP**, fast axis: -45°) before it impinged on the sample (**S**). The transmission diffraction pattern was received at the transmission side by a CCD camera (**CCD1**, provided by Nikon). In order to capture the diffraction pattern at the reflection side, we used a beam splitter (**BS**) and located it contact with the front surface of the sample cell to decrease the displacement of the diffraction beams, so that the diffraction pattern at the reflection side can be received by the other CCD (**CCD2**, provided by Nikon). As aforementioned, the refractive-index-matching layer was coated on the contact surface to avoid the Fresnel reflection at the interface induced by the beam splitter and sample cell.

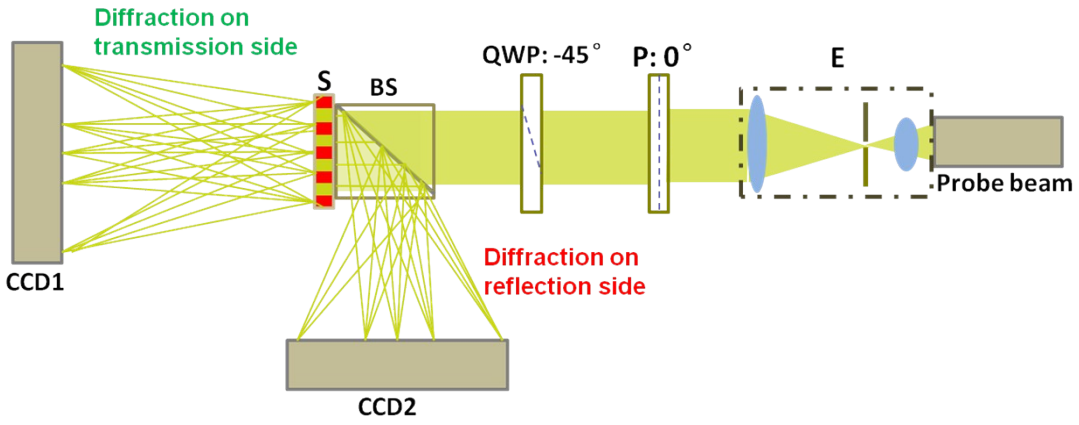

Fig. S3. Optical setup for detecting the diffraction patterns.

Additional discussions on the amplitude grating

The incident wavelength located between the reflection bands of two neighboring stripes

To demonstrate the diffraction when the wavelength of the impinged light located between the reflection bands of the adjacent exposed and unexposed areas, we tested the refractive indices (*i.e.*, the phase, φ, which has a relationship with refractive index, n, $\varphi=2\pi nd/\lambda$) of the two areas respectively under the normal incidence of the right-handed CPL with the aforementioned wavelength by interferometry, and followed by rechecking the diffraction in the corresponding situation. To the right-handed CPL incident light, the refractive index is denoted as n_L within the CLC with the long-wavelength reflection band and the other denoted as n_s with the short-

wavelength reflection band. By modulating the reflection bands of the exposed and unexposed areas, rendering the three wavelengths (~530nm, ~600nm and ~650nm) located between two reflection bands respectively, the refractive indices of n_L and n_S can be tested under these wavelengths. Our measured results indicated that the difference between n_L and n_s corresponding to the above three wavelengths was as small as 0.01, leading to a weak +1st-order diffraction with the efficiency of less than 2.0% which can be almost neglected and the efficiency of the 0th-order was 94.8% from the theoretical Eq. S3 and S4. To prove our theoretical analysis, we rechecked the diffraction patterns of the CLC grating with the 532-nm probe beam (as shown in the following Figure S4a). The corresponding wavelength is located between the reflection bands of the two areas. The tested diffraction efficiencies of '+1' and zero orders are 1.8% and 90.5% respectively, which are in good agreement with the calculated results. On the other hand, to the left-handed CPL incident light, the diffraction doesn't appear (as shown in Figure S4b), implying that there are not any phase difference between the two types of CLC areas. Therefore, we can confirm by combining the aforementioned theoretical and experimental results that the diffraction caused by the phase-differences between the exposed and unexposed areas is so small that can be almost neglected when the wavelength of probe beams lays between two reflection bands of two adjacent areas. Thus, it is reasonable to consider that the amplitude modulation between the two CLC areas is the main factor for the appearance of diffraction.

$$\Delta\varphi = \frac{2\pi}{\lambda}\Delta nd = \frac{2\pi}{\lambda}\left|n_s - n_L\right|d \qquad \text{Eq. (S3)}$$

$$\begin{cases} \eta_0 = 1 - 2\dfrac{l}{\Lambda}\left(1 - \dfrac{l}{\Lambda}\right)\left(1 - \cos\Delta\varphi\right) \\ \eta_n = \dfrac{1}{n^2\pi^2}\left(1 - \cos\Delta\varphi\right)\left(1 - \cos\dfrac{2\pi nl}{\Lambda}\right) \end{cases} \qquad \text{Eq. (S4)}$$

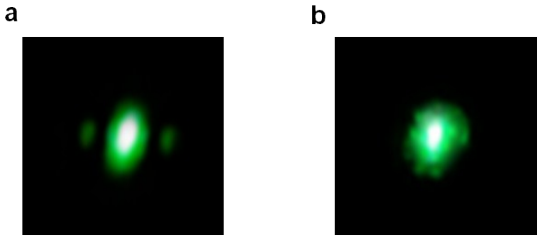

Fig. S4. Diffraction patterns with the (a) right-handed CPL and (b) left-handed CPL when the wavelength of impinged light lays in between the two reflection bands of neighboring stripes.

Calculation by scalar diffraction theory

The amplitude regime of the CLC grating can be confirmed in further through the scalar diffraction theory. Assuming a grating with amplitude modulation as well as the phase modulation, the complex amplitude distribution (*A*) of the diffraction pattern can be expressed as the Fourier transform in Eq. (S5); the diffraction intensity distribution is given in Eq. (S6); φ_0 in the two equations is phase difference. *a* is the width of single exposed or unexposed area; x_0 and *u* are the spatial coordinate and the spatial frequency coordinate. In the case of a 650-nm incident wavelength, the amplitude, A_1 and A_2 were the squire roots of the transmission intensities T_1, T_2, *i.e.*, $A_1 = \sqrt{T_1} \approx 0.9$ and $A_2 = \sqrt{T_2} \approx 0.3$ Thus the 0th-order and +1st-order diffraction efficiencies were

calculated as 36.0% and 3.6%, when the phase difference φ_0=0. The theoretical results were quite conformed to the experimental results, where the 0th-order and +1st-order diffraction efficiencies were tested as 36.9% and 3.5%. Therefore, from such comparison, we believe the CLC grating should be amplitude regime.

$$A(u)=\left[\int_0^a A_1\cdot\exp(-i2\pi ux_o)dx_o+\int_{-a}^0 A_2\cdot\exp(i\varphi_0)\exp(-i2\pi ux_o)dx_o\right]\frac{\sin(N\pi 2au)}{\sin(\pi 2au)} \qquad \text{Eq. (S5)}$$

$$I(u)=A(u)\cdot A^*(u)=\left[A_1^2+A_2^2+2A_1A_2\cos(2\pi ua+\varphi_0)\right]\left[a\sin c(au)\frac{\sin(N\pi 2au)}{\sin(\pi 2au)}\right]^2 \qquad \text{Eq. (S6)}$$

The missing order from the CLC grating with unsharp boundaries

Another phenomenon can prove the amplitude regime of the presented grating. Figure S5a shows the micro-pattern with diffused boundary obtained by irradiating the sample without pre-photo-crosslinking through a photomask, width-ratio between the exposed and unexposed areas is 1:1. The exposed area was labeled as "i" in the figure; the diffused areas were "ii" and "iii" and the unexposed area includes "ii", "iii" and "iv". The width of area "i" was almost equal to the total width of "ii", "iii" and "iv". We used 532-nm light (the wavelength was located in the reflection band of area "i" while out of area “ii”, “iii” and “iv”) as the probe light. Under the circumstance, if there existed evident phase differences among these areas "i", "ii", "iii" and "iv", the even diffraction orders would appear as the rectangular grating (*i.e.* binary distribution of the complex amplitude of incident light) is replaced by the multi phase distribution in one grating period. Otherwise, the missing even orders would occur because only the amplitude modulation is induced between the exposed (“i”) and unexposed (“ii”, “iii” and “iv”) areas, meeting the rectangular distribution of grating. From the experimental results shown in Figure S5b, the observed diffraction patterns with typical missing of the even diffraction orders proved that the effect of phase modulation on the diffraction was so weak that can be neglected. Therefore, such grating belongs to the amplitude regime.

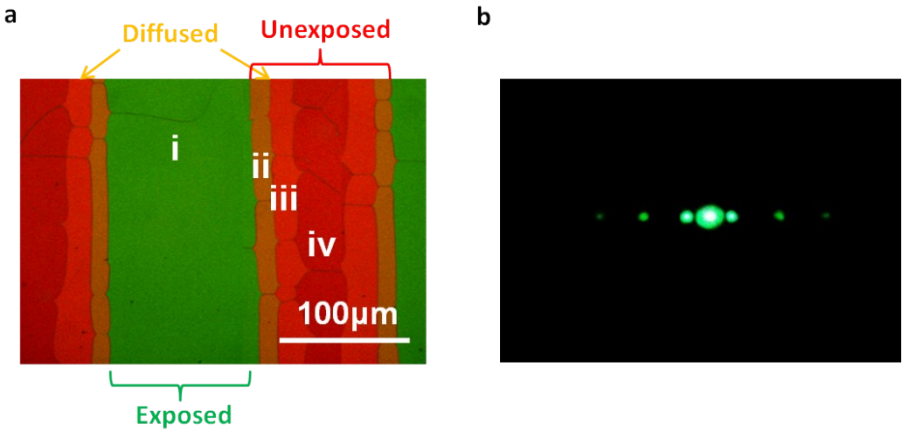

Fig. S5. (a) Texture of the CLC grating with the diffused boundaries, and (b) its corresponding diffraction pattern.

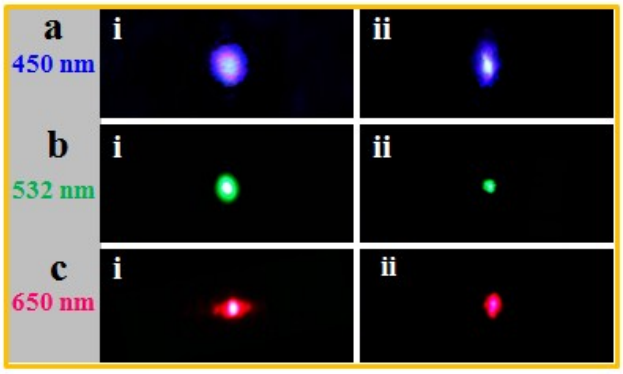

Fig. S6. Light patterns after impinging on the grating shown in Fig. 2c in the cases that (**a**) the wavelength mismatched with the grating; and (**b**), (**c**) the polarization was opposite to the handedness of CLCs. The incident wavelengths were given at the left side. Patterns on the transmission (**a**-i, **b**-i and **c**-i) and reflection (**a**-ii, **b**-ii and **c**-ii) sides were presented.

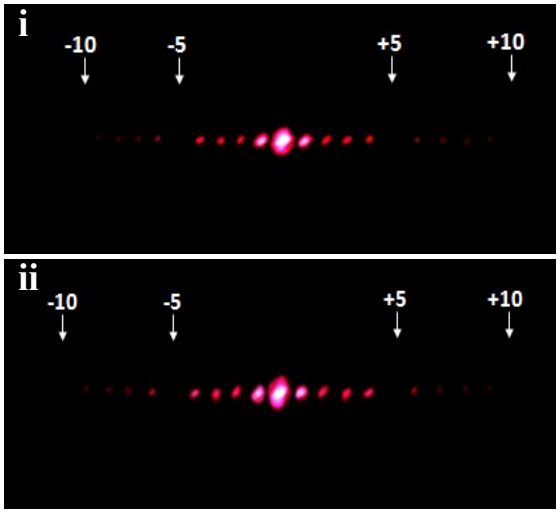

Fig. S7. Diffraction missing at *5n*th (*n* is an integer) orders both on the (i) transmission and (ii) reflection sides of the grating with a 4:1 or 1:4 width-ratio between the exposed and unexposed areas.

References

1. See Supporting Information of T. H. Lin, Y. Li, C. T. Wang, H. C. Jau, C. W. Chen, C. C. Li, H. K. Bisoyi, T. J. Bunning and Q. Li, *Adv. Mater.*, 2013, **25**, 5050.
2. See Supporting Information of Y. Li, C. Xue, M. Wang, A. Urbas and Q. Li, *Angew. Chem. Int. Ed.*, 2013, **125**, 13948.